Acta Geotechnica (2019) 14:329–345
https://doi.org/10.1007/s11440-018-0675-0

RESEARCH PAPER

A critical state constitutive model for clean and silty sand

X. Wei[1] · J. Yang[1]

Received: 4 November 2017 / Accepted: 30 April 2018 / Published online: 12 May 2018

Abstract

The mechanical behavior of silty sand is highly dependent on the percentage of fines in addition to the packing density and confining pressure. Properly modeling the diverse behavior of silty sand remains an area of difficulty and uncertainty. This paper presents an attempt to formulate a critical state-based constitutive model for sand with varying fines content based on several new laboratory findings. A marked feature of the model is a unified description of the state-dependent elastic modulus as well as a unified description of plastic hardening modulus such that only one set of elastic and hardening parameters is required for sand with different fines contents. The model is calibrated and validated using the results from a structured experimental program. It shows that the model can produce reasonably good predictions for undrained shear responses of sand specimens under a range of void ratios, confining stresses and fines contents. In particular, it successfully predicts the laboratory observation that under otherwise similar conditions, the presence of non-plastic fines increases the liquefaction susceptibility of sand.

Keywords Constitutive modeling · Critical state · Liquefaction · Silty sands · State parameter

List of symbols

A_e	Fitting parameter of G using $F(e)$
a_e	Fitting parameter of G in $F(e)$
A_ψ	Fitting parameter of G using $F(\psi)$
a_ψ	Fitting parameter of G in $F(\psi)$
C_0	Model parameter in C_r
C_r	Reduction factor for elastic shear modulus
D	Dilatancy
d_0	Dilatancy parameter
$d\varepsilon_q$	Deviatoric strain increment
$d\varepsilon_q^e$	Elastic deviatoric strain increment
$d\varepsilon_q^p$	Plastic deviatoric strain increment
$d\varepsilon_v$	Volumetric strain increment
$d\varepsilon_v^e$	Elastic volumetric strain increment
$d\varepsilon_v^p$	Plastic volumetric strain increment
e	Void ratio
e_0	Initial void ratio prior to shearing (i.e., post-consolidation void ratio e_c)
e_Γ	Intercept of critical state line (CSL) in the $e - (p'/P_a)^\xi$ plane
$F(e)$	Void ratio function
$f(X_1, X_2, X_3\ldots)$	Function of $X_1, X_2, X_3\ldots$
$F(\psi)$	State parameter function
FC	Fines content (%)
f_c	Fines content in decimal
G	Elastic shear modulus
h, h_1, h_2	Hardening parameters
K	Elastic bulk modulus
k	Pressure exponent of modulus
k_1	Model parameter in C_r
K_p	Plastic hardening modulus
L	Loading index
m	Dilatancy parameter
M	Stress ratio (η) at critical state
n	Hardening parameter
p'	Mean effective stress
$p_c{}'$	Post-consolidation pressure (i.e., initial mean effective stress)
P_a	Reference stress equaling to 1 atm
PSD	Particle size distribution
PTS	Phase transformation state
q	Deviatoric stress
R	Roundness of sand particle
R_{comb}	Combined roundness
UIS	Undrained instability state
α	Model parameter in K_p
ε_q	Deviatoric strain

✉ J. Yang
junyang@hku.hk

[1] Department of Civil Engineering, The University of Hong Kong, Hong Kong, China

ε_q^e	Elastic deviatoric strain
ε_q^p	Plastic deviatoric strain
ε_v	Volumetric strain
ε_v^e	Elastic volumetric strain
ε_v^p	Plastic volumetric strain
ζ	Accumulated plastic deviatoric strain
η	Stress ratio q/p'
η_{peak}	Stress ratio (η) at peak state
η_{PTS}	Stress ratio (η) at phase transformation state
λ_c	Magnitude of the slope of CSL
ν	Poisson's ratio
ξ	Pressure exponent of CSL formulation
φ_{cs}	Critical state friction angle
ψ	State parameter
ψ_0	Initial state parameter prior to shearing

1 Introduction

It is widely recognized that the mechanical behavior of sand is highly dependent on the packing density and confining pressure. The fines content (FC) is another important factor that can significantly alter the shearing resistance of sand. Several laboratory investigations have shown that the effect of fines can be either beneficial or detrimental [10, 18, 19, 21, 29, 41, 46]; the contradictory effects are partly due to the use of different density variables for comparison [42]. Based on a detailed investigation into the rationale of different density variables, Yang et al. [42] suggested that the usual global void ratio (e) remains a proper density variable as compared with the skeleton void ratio and the equivalent inter-granular void ratio. When compared at the same post-consolidation global void ratio, the presence of non-plastic fines is to increase the liquefaction potential of sand [41, 42], as shown in Fig. 1 for Toyoura sand mixed with crushed silica silt [42]. More recently, several laboratory studies have also found that the elastic shear modulus (G) of sand tends to decrease with the addition of non-plastic fines [32, 38]. The effects of fines along with the effects of density and confining stress make it difficult to characterize the behavior of silty sand of varying fines content.

As far as the elastic property is concerned, a noteworthy finding from recent experiments [38] is that the shear modulus can be described in a more rational way through a state parameter function, $F(\psi)$, instead of the traditional void ratio function $F(e)$. Here, the state parameter ψ, defined by Been and Jefferies [1] in the framework of critical state soil mechanics (CSSM), is a measure of how far the material state is from the critical state in terms of density. It has also been found that several key aspects of the sand behavior observed in the laboratory, including onset of flow liquefaction [36] and cyclic liquefaction resistance under symmetric and non-symmetric loading [40], can be characterized using the state parameter. A number of critical state-based constitutive models have adopted the state parameter to simulate the shear behavior of sand [2, 3, 8, 12, 28, 37, 44, 45]; calibration and validation of these models have been mainly based on test data on clean sand. When these models are applied to silty sands, FC-specific model parameters are generally required. This implies that a clean sand mixed with different percentages of fines need to be treated as different materials.

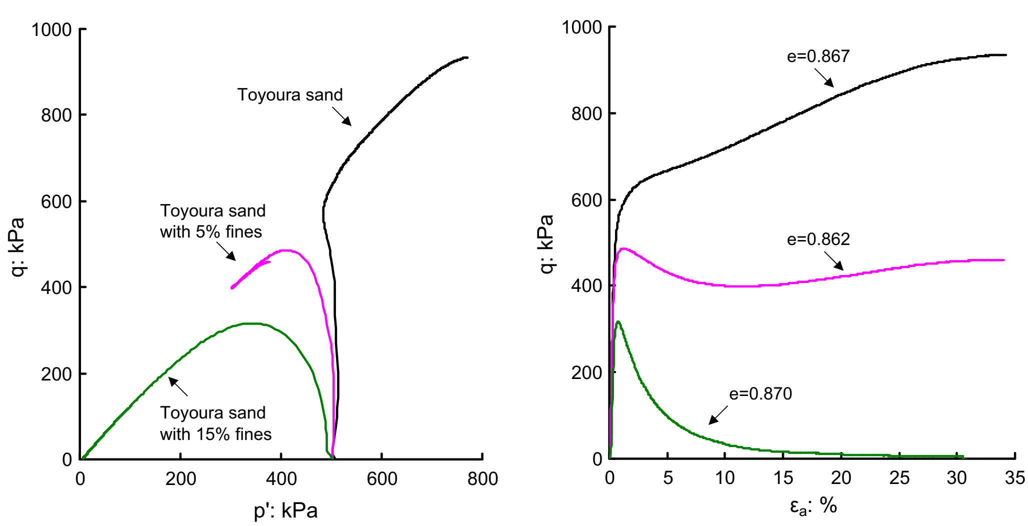

Fig. 1 Experimental observation on the effects of fines on the monotonic mechanical behaviors of sands and silty sands [42]

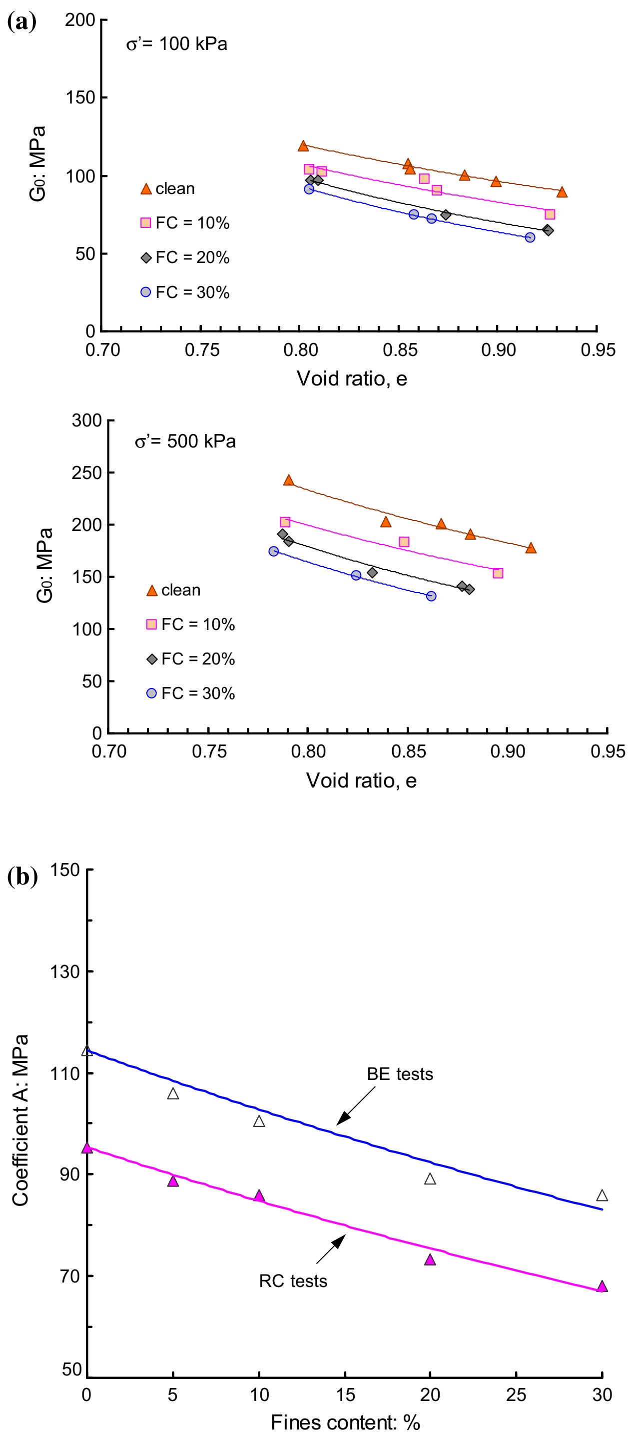

Fig. 2 **a** FC-specific *G*–*e* relationships (after [38]), **b** parameter A_e decreases with increasing fines content (after [38])

The elastic modulus is an essential element of any elastoplastic constitutive model and it affects the stress–strain relationship through the general stiffness matrix [22, 34]. A proper description of the elastic behavior of soils plays an important role in performance-based designs of geotechnical structures. This paper presents an attempt to formulate a simple constitutive model for sand with different quantities of fines, which incorporates the state-parameter dependence of elastic modulus, as observed in recent experiments, and a state-parameter-dependent plastic hardening modulus. Calibration and validation of the model are conducted using data sets from a structured experimental program on sand-fines mixtures.

2 Constitutive framework

For the sake of clarity, the model is formulated in the standard triaxial space using the platform of [12]. The yield surface $f(p, q, \eta)$ is given as:

$$f(p', q, \eta) = q - p'\eta = 0 \tag{1}$$

where p' is the mean effective stress, q is the deviatoric stress and η is the stress ratio. The loading index (L) is defined as:

$$L = \frac{1}{K_\mathrm{p}}\left(\frac{\partial f}{\partial q}\mathrm{d}q + \frac{\partial f}{\partial p'}\mathrm{d}p'\right) = \frac{1}{K_\mathrm{p}} p'\mathrm{d}\eta \tag{2}$$

where K_p is the plastic hardening modulus to be defined later. The non-associated flow rule is adopted to define the plastic strain increments as:

$$\begin{cases} \mathrm{d}\varepsilon_\mathrm{q}^\mathrm{p} = L = \dfrac{1}{K_\mathrm{p}} p'\mathrm{d}\eta \\ \mathrm{d}\varepsilon_\mathrm{v}^\mathrm{p} = LD = \dfrac{D}{K_\mathrm{p}} p'\mathrm{d}\eta \end{cases} \tag{3}$$

where $\mathrm{d}\varepsilon_\mathrm{q}^\mathrm{p}$ and $\mathrm{d}\varepsilon_\mathrm{v}^\mathrm{p}$ are the plastic deviatoric strain increment and the plastic volumetric strain increment, respectively, and D is the dilatancy. By assuming the additive decomposition of strain measurements, the following equations can be obtained:

$$\begin{Bmatrix} \mathrm{d}\varepsilon_\mathrm{q} \\ \mathrm{d}\varepsilon_\mathrm{v} \end{Bmatrix} = \begin{bmatrix} \dfrac{1}{3G} + \dfrac{1}{K_\mathrm{p}} & -\dfrac{\eta}{K_\mathrm{p}} \\ \dfrac{D}{K_\mathrm{p}} & \dfrac{1}{K} - \dfrac{D\eta}{K_\mathrm{p}} \end{bmatrix} \begin{Bmatrix} \mathrm{d}q \\ \mathrm{d}p' \end{Bmatrix} \tag{4}$$

Reversing Eq. (4) gives the general elastoplastic constitutive relationship as follows:

$$\begin{Bmatrix} \mathrm{d}q \\ \mathrm{d}p' \end{Bmatrix} = \left(\begin{bmatrix} 3G & 0 \\ 0 & K \end{bmatrix} - \frac{h(L)}{K_\mathrm{p} + 3G - K\eta D} \times \begin{bmatrix} 9G^2 & -3KG\eta \\ 3KGD & -K^2\eta D \end{bmatrix} \right) \begin{Bmatrix} \mathrm{d}\varepsilon_\mathrm{q} \\ \mathrm{d}\varepsilon_\mathrm{v} \end{Bmatrix}. \tag{5}$$

2.1 Implementation of CSSM

2.1.1 Elastic moduli

The following equation has been widely used to describe the elastic shear modulus for sand [7, 32]:

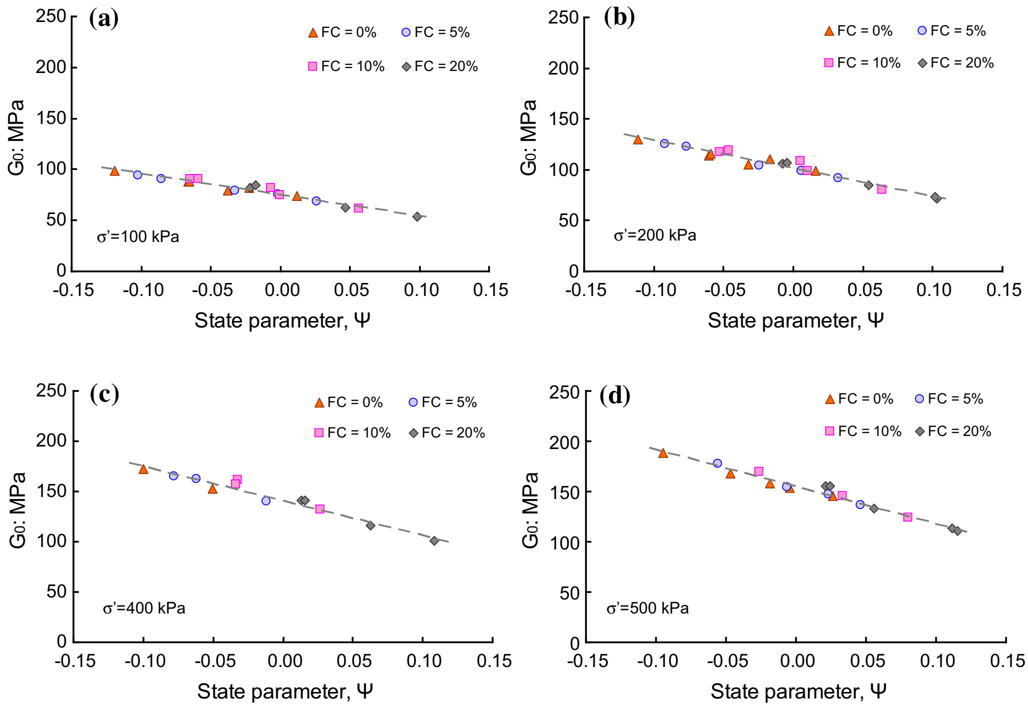

Fig. 3 FC-unified elastic G–ψ relationship for different confining pressures: **a** $p' = 100$ kPa, **b** $p' = 200$ kPa, **c** $p' = 400$ kPa, **d** $p' = 500$ kPa (after [38])

$$G = A_e F(e)\left(\frac{p'}{P_a}\right)^k = A_e \frac{(a_e - e)^2}{1 + e}\left(\frac{p'}{P_a}\right)^k \tag{6}$$

where A_e, a_e and k are fitting parameters, P_a is the atmospheric pressure. Laboratory studies using the bender element or resonant column technique have found that the addition of non-plastic fines to clean sand can alter the elastic stiffness of sand [33, 38], as shown in Fig. 2a for clean Toyoura sand mixed with different percentages of silica silt. It is clear that when compared at the same post-consolidation void ratio and confining stress, the elastic shear modulus (G) decreases with increasing fines content (up to a threshold fines content of $\sim$ 30%). This implies that a constitutive model using the traditional void ratio formulation of elastic modulus given in Eq. (6) requires FC-specific model parameters. Even after the G values are corrected by a void ratio function, e.g., $F(e) = (2.17 - e)^2/(1 + e)$, the parameter A_e remains a function of FC, as shown in Fig. 2b.

When measured G values are plotted as a function of the state parameter (ψ) corresponding to the post-consolidation state, the effect of fines content can be unified such that G values decrease with increasing ψ in a consistent manner, as shown in Fig. 3. This significant finding eventually leads to a state-parameter-dependent elastic shear modulus as follows [38]:

$$G = A_\psi F(\psi)\left(\frac{p'}{P_a}\right)^k = A_\psi \frac{(a_\psi - \psi)^2}{1 + \psi}\left(\frac{p'}{P_a}\right)^k \tag{7}$$

where A_ψ, a_ψ and k are fitting parameters. Yang and Liu [38] have shown that the notion of ψ-dependent shear modulus applies to different sand-fines mixtures including a natural silty sand [6].

The elastic bulk modulus, K, can be obtained by measuring the compressional wave velocity, and a similar state-parameter dependence of K is anticipated. Alternatively, K can be estimated by the following relation:

$$K = G\frac{2(1 + v)}{3(1 - 2v)} \tag{8}$$

where v is Poisson's ratio. If the common assumption of constant v is adopted, then a state-parameter-dependent K is straightforward.

2.1.2 Dilatancy

The dilatancy, D, is given as follows [12]:

$$D = \frac{d_0}{M}[M\exp(m\psi) - \eta] \tag{9}$$

where d_0 and m are model parameters. The above equation indicates a state-dependent flow rule.

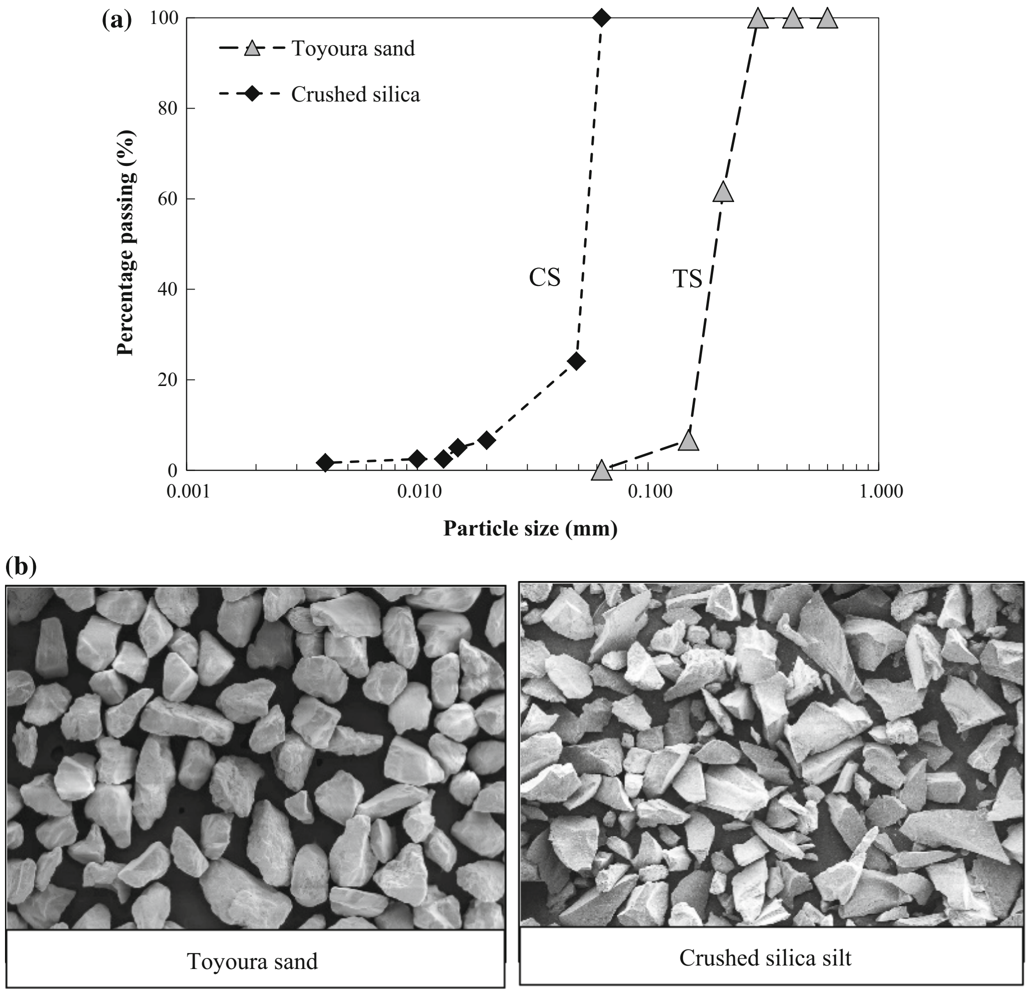

Fig. 4 Toyoura sand and crushed silica silt for laboratory tests. **a** Particle size distribution, **b** SEM images of the materials

Table 1 Undrained triaxial tests for calibration [15]

Test ID	FC (%)	e_c^a	p_c': kPa[a]	ψ_0^a
TS-IC015	0	0.928	500	0.044
TS-IC016	0	0.894	500	0.010
TS-IC017	0	0.878	500	− 0.006
TSS10-IC007	10	0.880	300	0.037
TSS10-IC009	10	0.880	500	0.062
TSS10-IC010	10	0.901	500	0.083
TSS20-IC007	20	0.846	500	0.082
TSS20-IC010	20	0.834	300	0.043

[a]After consolidation and before shearing

2.1.3 Plastic hardening modulus

The plastic hardening modulus, K_p, is given below to capture the softening response of sand:

$$K_p = \frac{hG\exp(n\psi)}{\eta}[M\exp(-n\psi) - \eta] \quad (10)$$

where h and n are model parameters. The parameter h is a hardening parameter that was originally proposed as a function of the initial void ratio as [11]

$$h = h_1 - h_2 e_0 \quad (11)$$

where h_1 and h_2 are two positive fitting parameters. Li [11] mentioned that the state parameter may not be used for h because an increase in state parameter can be achieved by either increasing the void ratio or the effective stress. However, an increased void ratio may decrease K_p, whereas an increased effective stress may increase K_p. In other words, a change of state parameter ($\Delta\psi$) can cause ambiguous effects on K_p if $\Delta\psi$ corresponds to changes in void ratio and effective stress at the same time. Similarly, opposite effects exist for the state-parameter-dependent G as described in Eq. (7), but the effects are minor. This is probably because the effect of effective stress on K_p or

Table 2 Calibrated parameters for moist-tamped Toyoura sand mixed with crushed silica silt

Critical state				Elastic		Dilatancy		Hardening	
FC	0	10%	20%						
e_Γ	0.9427	0.9117	0.8657	A_ψ (kPa)	41,330	d_0	*	h_1	3.72
λ_c	0.0225	0.0357	0.0388	a_ψ	1.36	m	**	h_2	29.78
				k	0.4				
ξ	0.6	0.6	0.6	C_0	0.6			n	1.1
M	1.21	1.24	1.29	k_1	2			α	500
				ν	0.2				

*d_0 = 0.65 for clean Toyoura sand, 0.6 for TSS10, and 0.55 for TSS20

**m = 3.5 for clean Toyoura sand, 2.5 for TSS10, and 2.0 for TSS20

G through state parameter is minor when compared with that through the exponential term of the effective stress, $(p'/P_a)^k$. Thus, the parameter h may be given as a function of the initial state parameter (ψ_0) as follows:

$$h = h_1 - h_2\psi_0 \tag{12}$$

where values of h_1 and h_2 are different from those in Eq. (11). In the next section, the state-parameter dependence of h will be verified using test data.

To incorporate the effects of accumulated plastic strain on the plastic hardening modulus and to facilitate the simulation of the undrained cyclic response of sand [30], K_p may be further modified as follows:

$$K_p = \frac{1}{1+\alpha\zeta}\frac{hG\exp(n\psi)}{\eta}[M\exp(-n\psi)-\eta] \tag{13}$$

where α is a positive fitting parameter, and ζ is the accumulated plastic deviatoric strain to be calculated using the following equation:

$$\zeta = \int \left|d\varepsilon_q^p\right|. \tag{14}$$

3 Model calibration

The model parameters are calibrated based on a series of laboratory tests on mixtures of Toyoura sand and crushed silica fines [15, 38]. The particle size distribution curves and SEM images of the base sand and the silica fines are shown in Fig. 4. In the laboratory tests, the specimens were prepared by the moist tamping method. The tests used for calibration of the constitutive model are listed in Table 1, and the calibrated parameters are summarized in Table 2.

3.1 Critical state parameters

The critical state parameters can be obtained from a series of monotonic triaxial tests. The critical state line in the e–p' plane is represented by a power law as [14, 16, 37]:

$$e = e_\Gamma - \lambda_c\left(\frac{p'}{P_a}\right)^\xi \tag{18}$$

where e_Γ is the intercept in the $e - (p'/P_a)^\xi$ plane, λ_c is the magnitude of the slope, and ξ is the pressure exponent (with a typical value ranging from 0.6 to 0.8, see [14]). The e_Γ and λ_c of sand-fines mixtures were found to be functions of fines content [41], as shown in Fig. 5, and can thus be estimated by some empirical methods [25] after the critical state line of the base sand is determined. The exponent ξ is taken as 0.6 in this study, which is the best-fitted value based on the test data of [15, 31].

The critical state stress ratio, M, can be readily determined from stress paths in the q–p' plane. The critical state friction angle (φ_{cs}) is largely affected by the roundness (R) of sand particles [39]. The concept of combined roundness [41], as defined below, can be adopted to characterize φ_{cs} of silty sand:

$$R_{comb} = R_{sand}\cdot(1-f_c) + R_{fines}\cdot f_c \tag{19}$$

where f_c is the fines content in decimal. The above relation implies that, for a given series of sand-fine mixtures (and hence similar shapes of coarse and fine particles), M is generally a function of fines content (Fig. 5).

3.2 Elastic properties

Theoretically, the elastic shear modulus [Eq. (7)] should be calibrated using experimental measurements at very small strains. However, the common practice for elastic modulus calibration is using the overall stress–strain relationship from triaxial tests, and this may lead to the calibrated

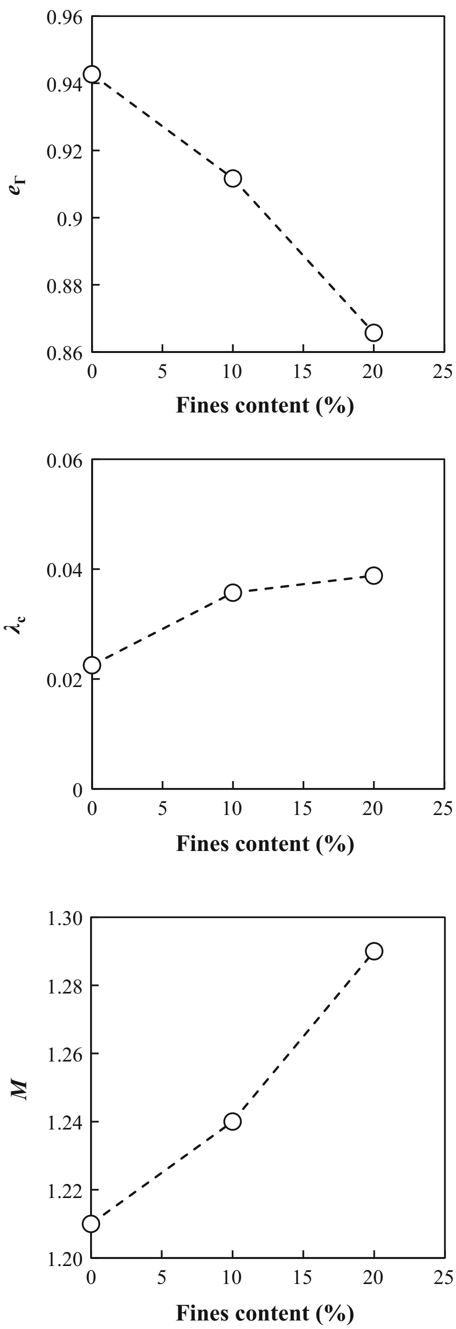

Fig. 5 Calibrated critical state parameters

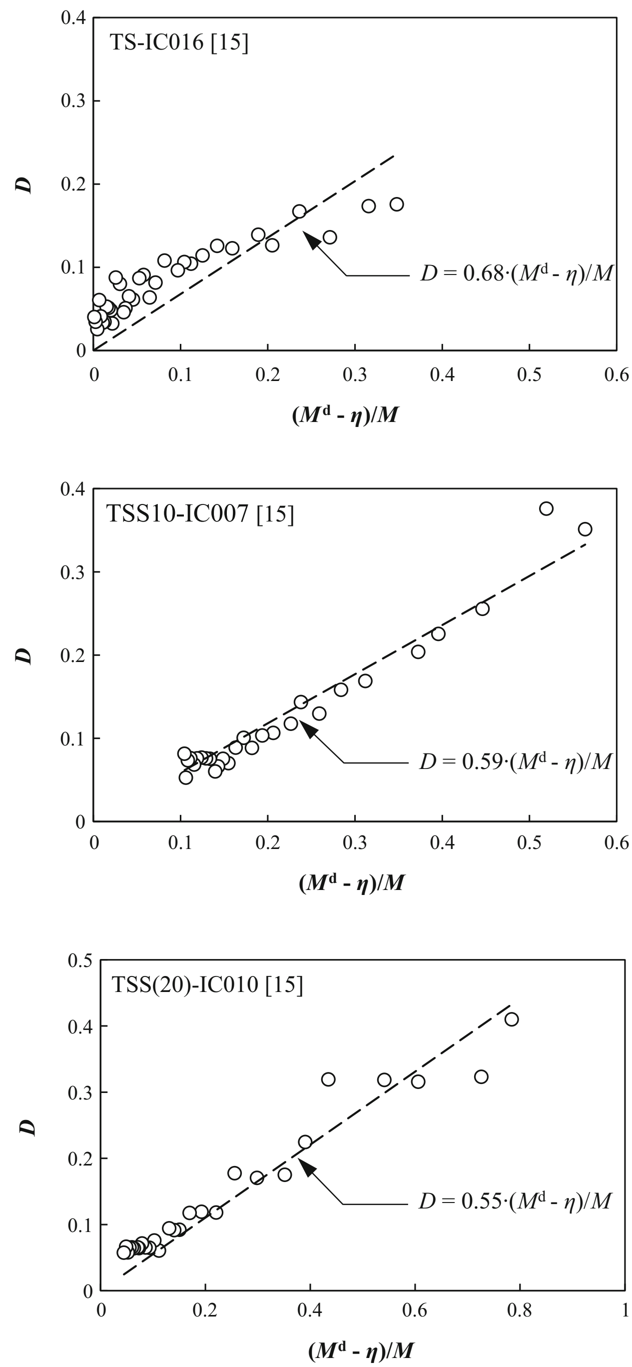

Fig. 6 Calibration of the dilatancy parameter d_0

elastic modulus being much lower than the measurements using dynamic methods such as bender element or resonant column tests. For example, the elastic shear modulus of Toyoura sand was calibrated using conventional triaxial test data [12] and the strain level involved in the calibration is around 10^{-4} [28]. This explains why the elastic modulus in these studies is quite lower than that measured by Yang and Liu [38] using the resonant column tests (Table 2). In general, use of the elastic shear modulus determined by dynamic methods can result in a very stiff stress–strain response and the attainment of characteristic states, such as phase transformation state or instability state, occurs at relative small strain levels. Dafalias and co-workers [17, 20] also noted this problem and suggested to reduce the shear modulus from small-strain measurements by a factor of 2–3. In this study, a reduction factor as given

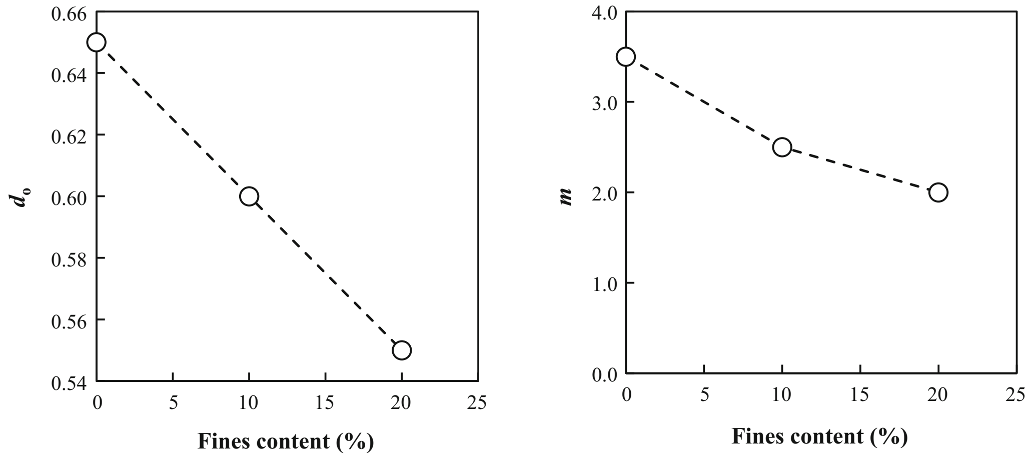

Fig. 7 Calibrated dilatancy parameters

below is applied, which takes into consideration the observed effect of stress ratio on the elastic shear modulus:

$$C_r = 1 - C_0\left(\frac{\eta}{\eta_{peak}}\right)^{k_1} \quad (20)$$

where C_0 is a positive parameter less than 1, and k_1 is also a positive parameter. The value of C_0 can be obtained by trial and error to fit the stress–strain response of the test data. The value of k_1 can be taken as a fixed value of 2.

Similarly, the elastic bulk modulus K can be calibrated by measuring the compressional wave velocity or using the isotropic compression tests. In this study, K is determined using Eq. (8) with the assumption of constant Poisson's ratio. Gu et al. [4] reported that the Poisson's ratio of Touyora sand ranges from 0.2 to 0.25 depending on void ratio and mean effective stress. For simplicity, the Poisson's ratio is assumed here to be a constant.

3.3 Dilatancy parameters

The dilatancy parameter m in Eq. (9) can be determined for $D = 0$ at the phase transformation state (PTS), where $\eta = \eta_{PTS}$. Therefore, m can be solved as follows:

$$m = \frac{1}{\psi_d}\ln\left(\frac{\eta_{PTS}}{M}\right) \quad (18)$$

where ψ_d is the state parameter at PTS. The value of m may vary for different fines contents [15, 18].

The dilatancy parameter d_0 can be determined by drained triaxial tests as suggested by [12] or by undrained triaxial tests if the incremental plastic strains are calculated as follows:

$$d\varepsilon_q^p = d\varepsilon_q - \frac{dq}{3G} \quad (19a)$$

$$d\varepsilon_v^p = d\varepsilon_v - \frac{dp'}{G}\frac{3(1-2v)}{2(1+v)} \quad (19b)$$

Then, the value of d_0 is obtained by fitting the D and $[(M^d - \eta)/M]$ as given below (Fig. 6):

$$D = d_0\frac{M\exp(m\psi) - \eta}{M} \quad (20)$$

The value of d_0 may vary slightly for a given fines content, and an average value is adopted (Table 2). The dilatancy relationship for sand seems to depend on particle shape and gradation (including fines content) [5, 24, 35]. Since there is a lack of experimental data for characterization of this dependency, the FC-specific dilatancy parameters d_0 and m are used in the present model (Fig. 7). Possible improvement in this regard may be made when more data are available.

3.4 Hardening parameters

The parameter n can be determined by the following equation, which is derived from $K_p = 0$ when the peak stress ratio state is attained ($\eta = \eta_{peak}$) during a drained triaxial test:

$$n = \frac{1}{\psi_{peak}}\ln\left(\frac{M}{\eta_{peak}}\right) \quad (21)$$

where ψ_{peak} is the state parameter at peak state. Because it has a minor effect on the simulation results, the parameter n is chosen as a constant independent of fines content.

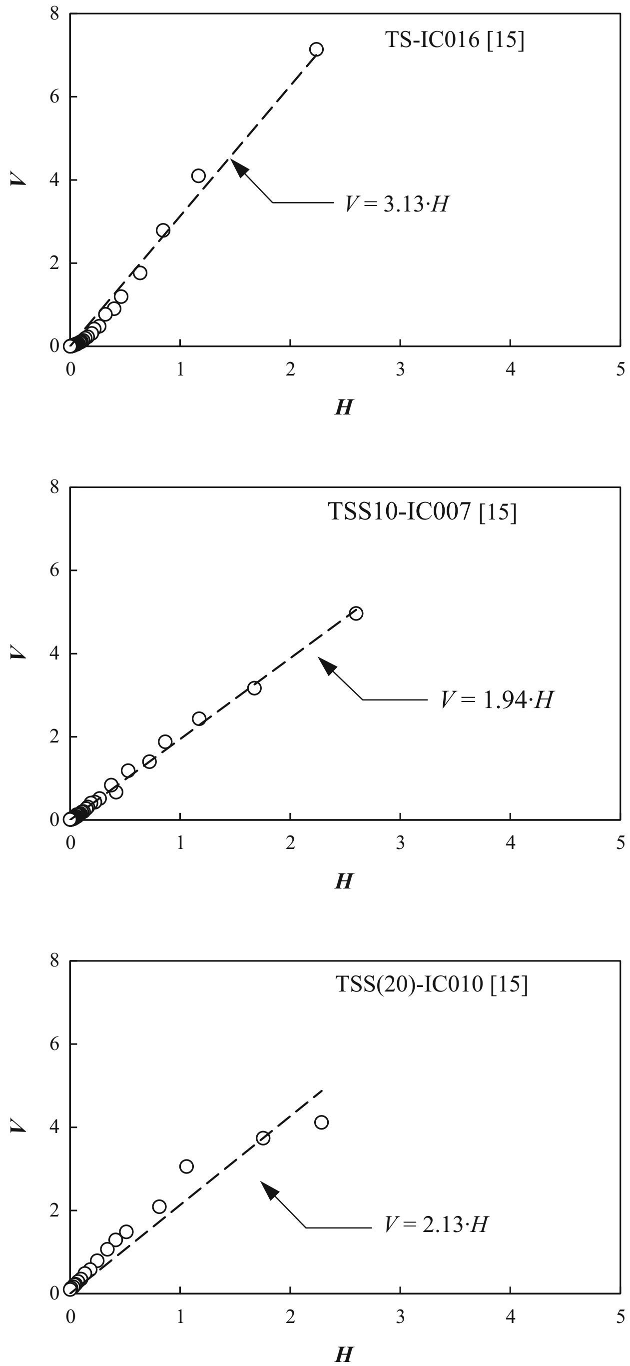

Fig. 8 Calibration of hardening parameter h

The parameter h can be determined by either drained or undrained triaxial tests [12]. Using undrained triaxial tests, it can be obtained by solving the following equation:

$$\frac{dq}{dp'} = \eta - \frac{h}{d_0} \frac{M \exp(n\psi)}{\eta} \frac{M \exp(-n\psi) - \eta}{M \exp(m\psi) - \eta} \frac{3(1-2v)}{2(1+v)} \quad (22)$$

Rearranging Eq. (22) into the following form:

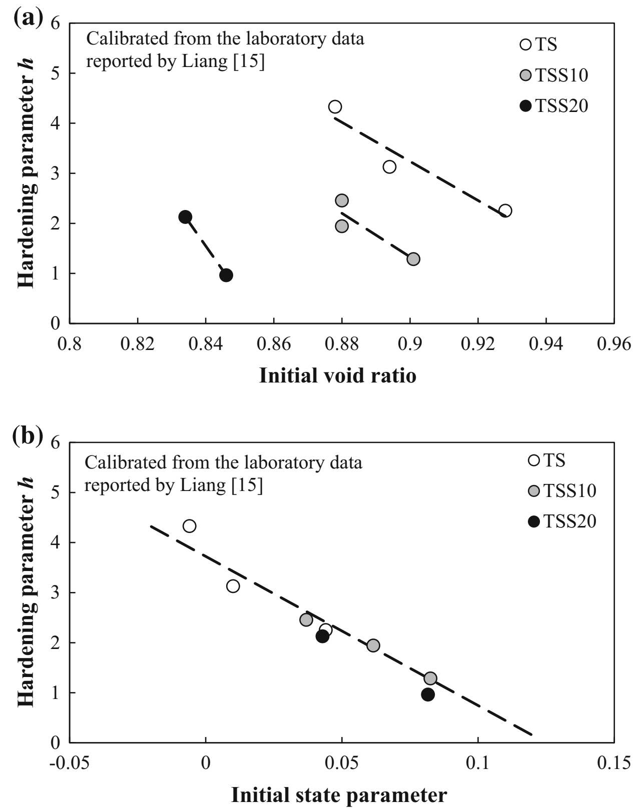

Fig. 9 Parameter h as a function of **a** the initial void ratio and **b** the initial state parameter

$$V = h \cdot H \quad (23)$$

where

$$V = \left(\eta - \frac{dq}{dp'}\right) \frac{d_0}{M} [M \exp(m\psi) - \eta] \frac{2(1+v)}{3(1-2v)} \quad (24)$$

$$H = \frac{\exp(n\psi)}{\eta} [M \exp(-n\psi) - \eta] \quad (25)$$

Parameter h can then be determined by plotting V against H (Fig. 8). Clearly, this hardening parameter decreases with increasing void ratio as shown in Fig. 9a, exhibiting different h–e relationships for different fines contents. It is also interesting to note the unified trend between h and the initial state parameter that the parameter h decreases with increasing initial state parameter (Fig. 9b). This trend is independent of fines content. The effects of initial effective confining pressure seem to be negligible, since the calibrated values of h are from tests with different initial effective stresses. This suggests a state-parameter dependence of parameter h that involves only a single set of h_1 and h_2. In this regard, both the elastic modulus and the plastic hardening modulus are state-parameter dependent and unified for different fines contents.

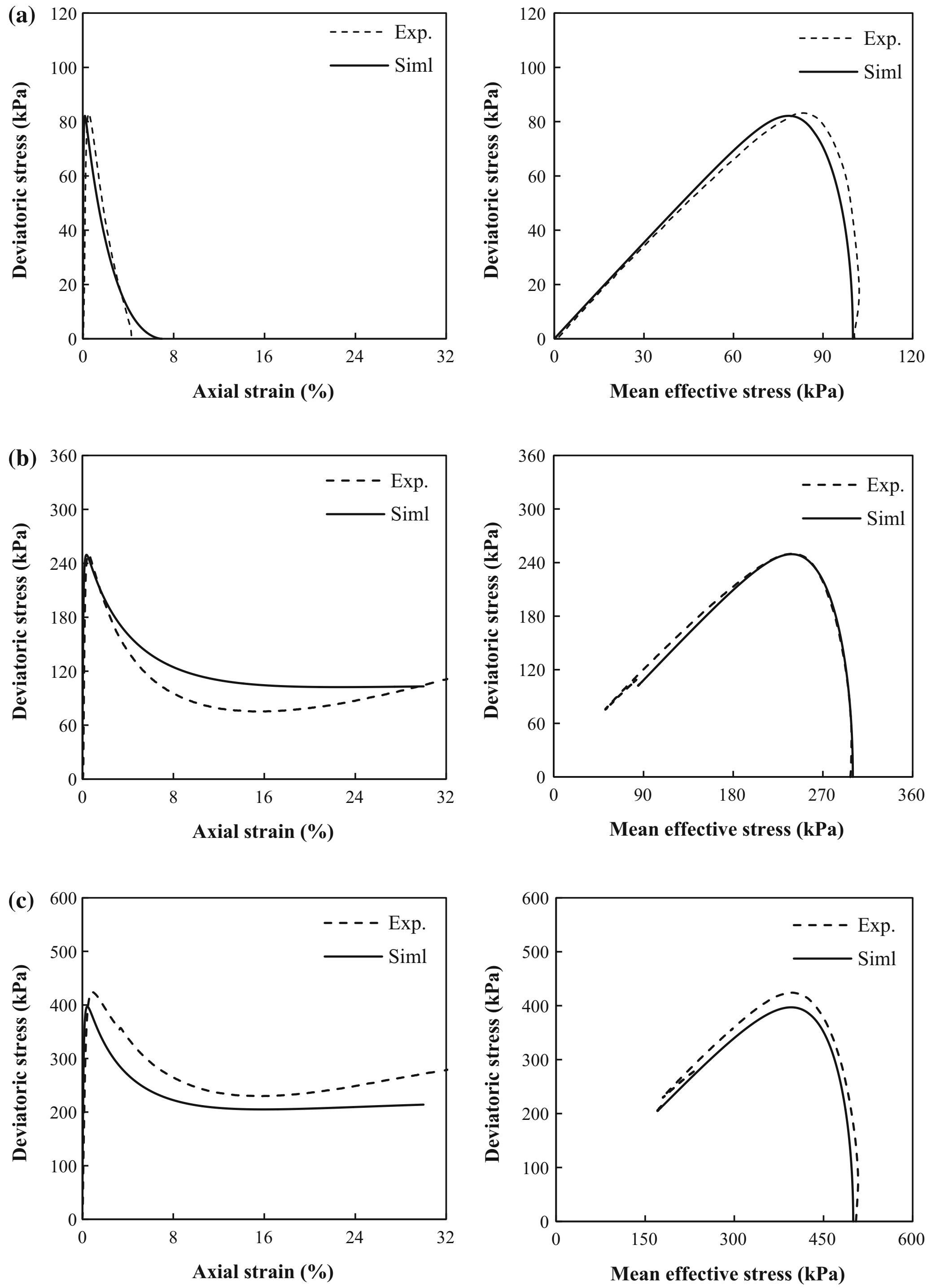

Fig. 10 Simulated flow type behavior of clean Toyoura sand compared with experimental data. **a** TS-IC002, $e_c = 0.951$, $p_c' = 100$ kPa, **b** TS-IC014, $e_c = 0.922$, $p_c' = 300$ kPa, **c** TS-IC011, $e_c = 0.910$, $p_c' = 500$ kPa

4 Simulations

The calibrated parameters in Table 2 are used to predict the undrained response of sand specimens with different fines contents and under various initial conditions. In Figs. 10, 11 and 12, the simulated results are compared with the test data reported by Liang [15] for specimens with FC = 0, 10, and 20%. Because the dilatancy parameters and the critical state parameters are only calibrated for three given FC (Figs. 5, 7), and because of the lack of extra data, a linear

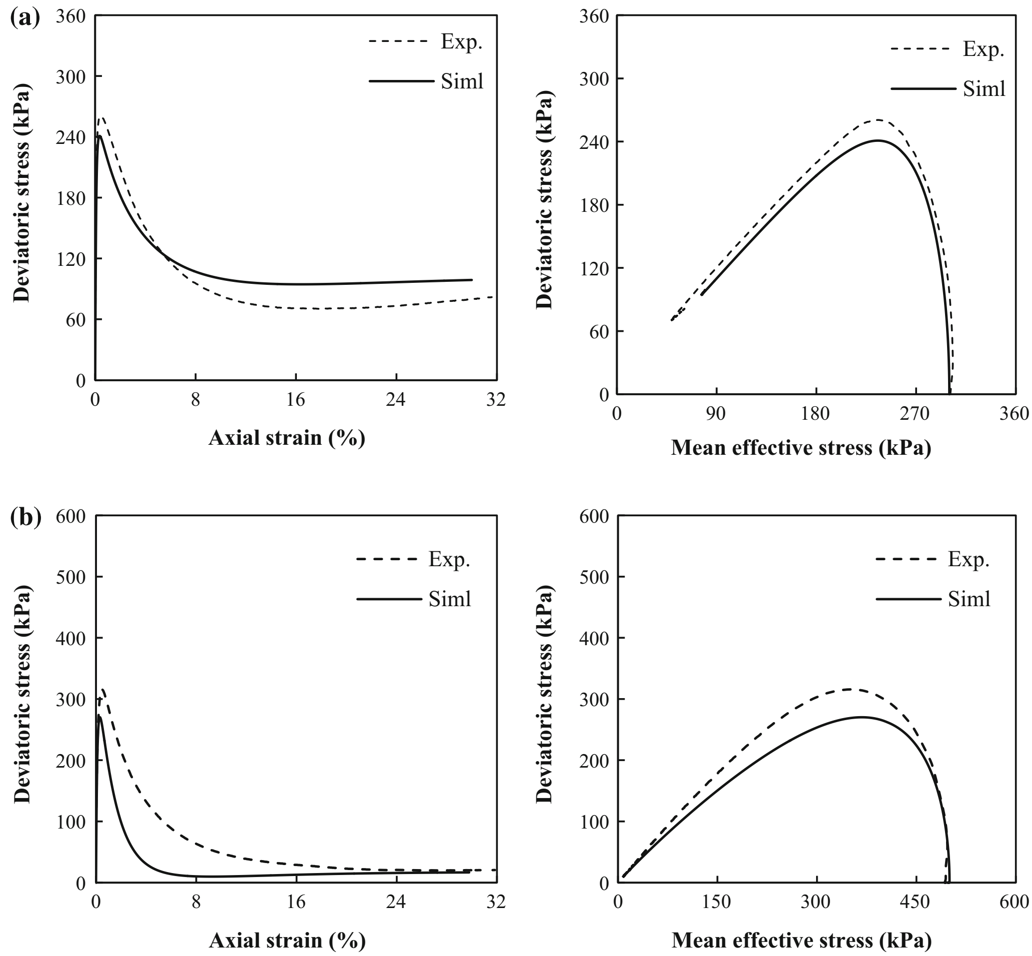

Fig. 11 Simulated flow type behavior of TSS10 compared with experimental data. **a** TSS10-IC007, e_c = 0.880, p_c' = 300 kPa, **b** TSS10-IC010, e_c = 0.901, p_c' = 500 kPa

interpolation is used to obtain the parameters for other fines contents. In Fig. 13, three undrained monotonic triaxial tests for FC = 5 and 15% reported by Yang et al. [42] are compared with the simulations. Table 3 includes the testing information of the undrained triaxial tests used for model validation.

In general, undrained monotonic behavior of clean and silty sands can be categorized into two major types [15, 26], namely flow type behavior (contractive behavior) and non-flow type behavior (dilative behavior). The flow type behavior is characterized by an instability state (i.e., undrained peak deviatoric stress state), and may exhibit several other different features, such as the quasi-steady state, depending on the density and initial effective stress. The non-flow type behavior does not have the undrained instability state nor the quasi-steady state. Nevertheless, it may have a phase transformation state before the critical state is attained. More detailed categorization and description of the various behavior of sand are given in [15, 26, 40].

4.1 Prediction of flow type behavior

The predicted flow type behavior is compared with the test data in Figs. 10, 11, 12 and 13, for fines content ranging from 0 to 20%. Note that the laboratory tests covered a wide range of initial void ratio (from 0.787 to 0.951) and a wide range of initial effective stress (from 100 to 500 kPa). The predicted stress–strain curves, as well as the effective stress paths, agree well with the test results. All simulation results and test data exhibit the undrained instability state and can thus be categorized as the flow type behavior.

Comparing the behavior in Fig. 10b, c for clean Toyoura sand (TS), the two specimens have different initial states in term of e and p', but they exhibit similar undrained response. This is reasonable as the initial state parameters for the two specimens (Table 3) are similar (0.026 for TS-

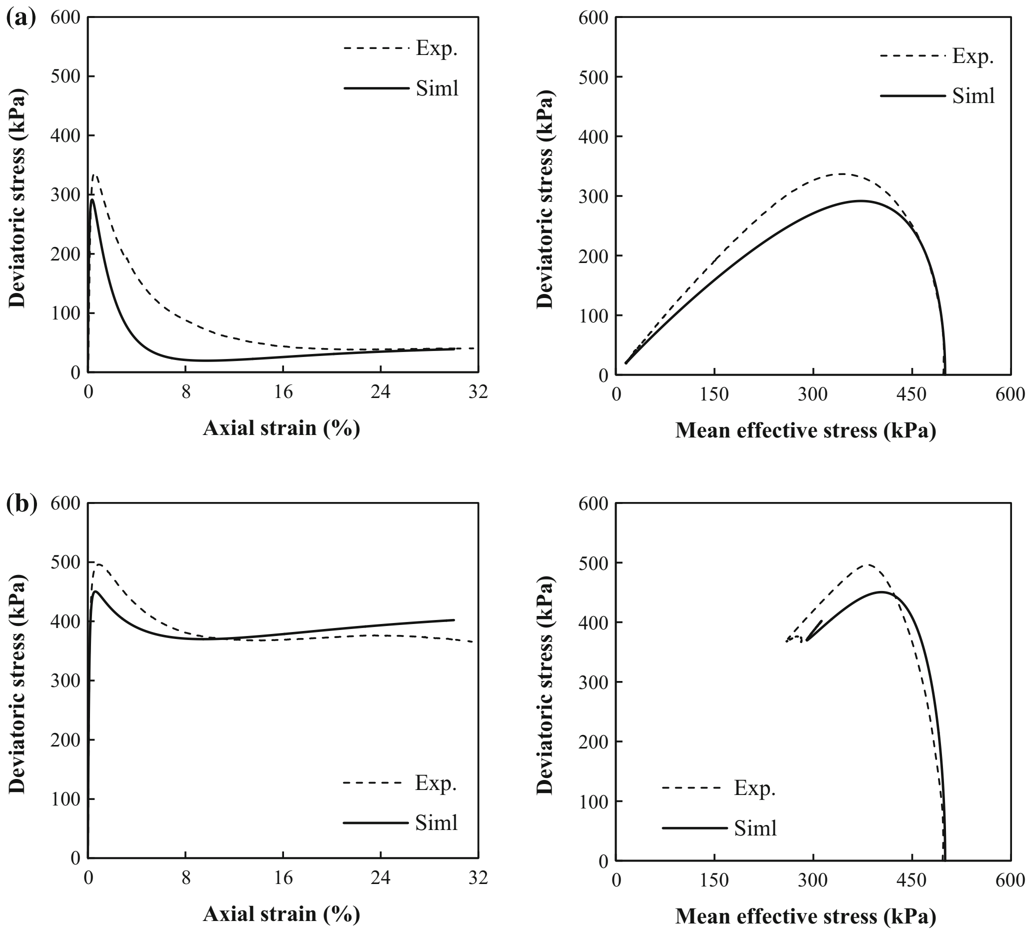

Fig. 12 Simulated flow type behavior of TSS20 compared with experimental data. **a** TSS20-IC007, $e_c = 0.846$, $p_c' = 500$ kPa, **b** TSS20-IC008, $e_c = 0.787$, $p_c' = 500$ kPa

IC011 and 0.023 for TS-IC014). Overall, the simulated results agree well with the laboratory observations. Specimens presented in Fig. 11b for TSS10 and Fig. 12a for TSS20 behave similarly too, but they have different fines contents (10 vs. 20%). Note that the two specimens have different initial states in term of e and p', but their initial same state parameters are almost the same (0.083 for TSS10-IC010 and 0.082 for TSS20-IC007). The test results indicate that undrained responses of specimens with different fines contents are primarily controlled by their initial state parameters and a similar initial state tends to result in a similar undrained response regardless of fines content. This state-parameter dependency of silty sand is well captured by the proposed constitutive model.

4.2 Prediction of non-flow type behavior

Three laboratory tests with fines content ranging from 0 to 20% are selected to validate the model for non-flow type behavior. The comparison between test results and simulations is presented in Fig. 14. The non-flow type behavior is characterized by pure dilative response with or without phase transformation state. Theoretically, the critical state is attained when the stress, pore water pressure and volumetric strain become constant with increasing shearing strain. In real laboratory tests, this ideal condition may be difficult to achieve for dilative specimens [9]. In this connection, some discrepancies may be observed between simulated and observed stress–strain curves. Nevertheless, the overall agreement is considered acceptable.

4.3 Predicting the effects of fines

Laboratory tests have confirmed that, when comparison is made at the same post-consolidation void ratio, the addition of non-plastic fines to clean sand can increase the liquefaction susceptibility to sand [42]. The constitutive model can successfully predict this important effect, as shown in Fig. 15. Three synthetic simulations, with FC =

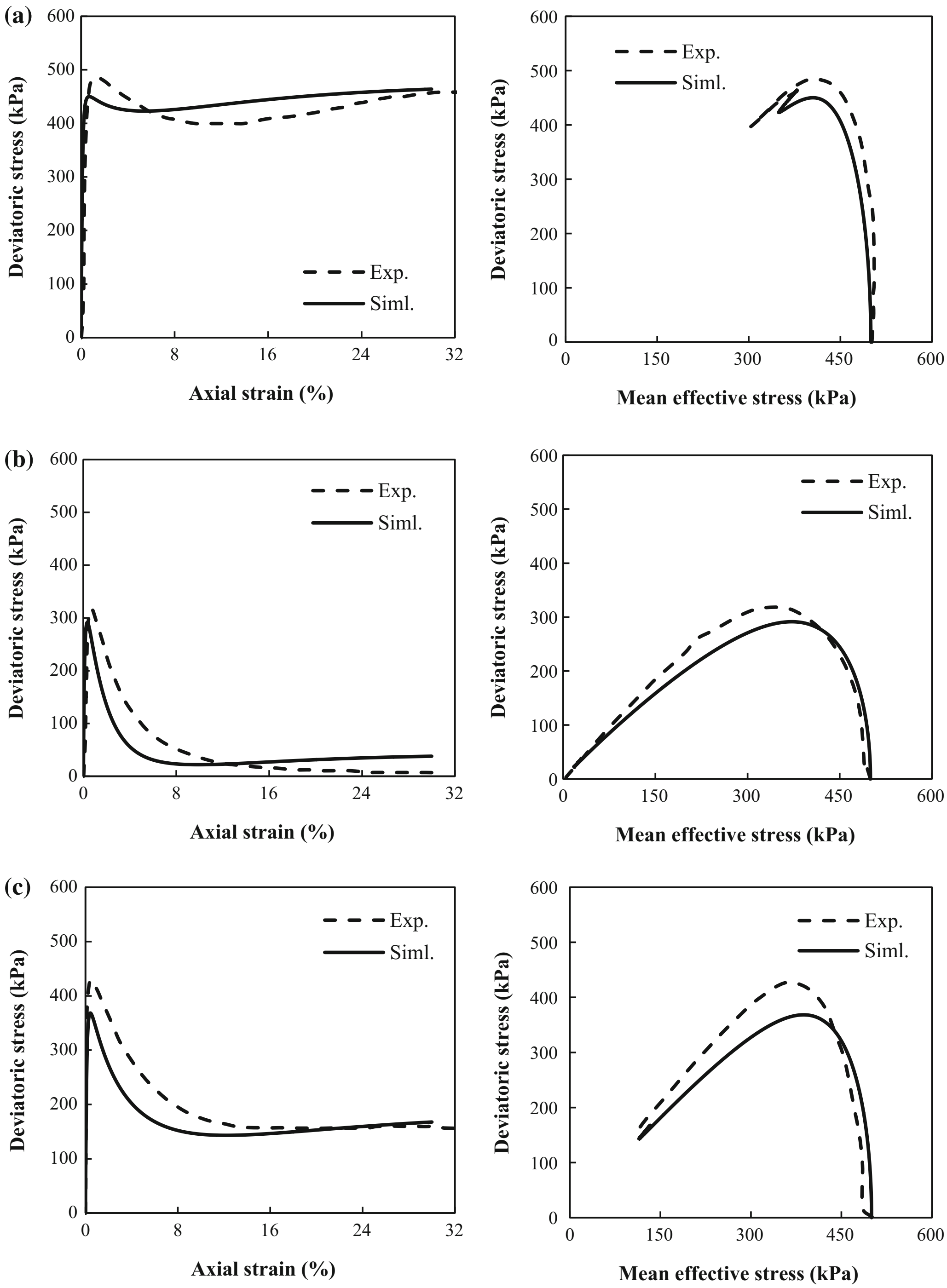

Fig. 13 Simulated flow type behavior of TSS5 and TSS15 compared with experimental data. **a** TSS5-IC005, $e_c = 0.862$, $p_c' = 500$ kPa, **b** TSS15-IC006, $e_c = 0.870$, $p_c' = 500$ kPa, **c** TSS15-IC002, $e_c = 0.842$, $p_c' = 500$ kPa

0, 10 and 20%, are performed to show the effects of fines at the initial state of $e_c = 0.880$ and $p_c' = 500$ kPa. The simulated TS specimen exhibits non-flow type failure as no undrained instability state occurs. On the contrary, flow type failure takes place when 10% fines are added to the sand. Furthermore, complete liquefaction occurs at the

Table 3 Undrained triaxial tests for validation [15, 42]

Test ID	FC (%)	e_c	p_c' (kPa)	ψ_0
Flow type				
TS-IC002	0	0.951	100	0.031
TS-IC011	0	0.910	500	0.026
TS-IC014	0	0.922	300	0.023
TSS5-IC005	5	0.862	500	0.011[a]
TSS10-IC007	10	0.880	300	0.037
TSS10-IC010	10	0.901	500	0.083
TSS15-IC002	15	0.842	500	0.051[a]
TSS15-IC006	15	0.870	500	0.079[a]
TSS20-IC007	20	0.846	500	0.082
TSS20-IC008	20	0.787	500	0.023
Non-flow type				
TS-IC008	0	0.867	100	− 0.053
TSS10-IC006	10	0.783	100	− 0.093
TSS20-IC004	20	0.788	100	− 0.039

[a]Initial state parameter calculated based on interpolated critical state lines

fines content of 20%. Note that the initial states of the three specimens are the same in terms of void ratio and effective stress. This implies that the initial state parameter increases with increasing FC because of the downward shift of the critical state line [41, 42]. The differences in initial state parameters are thought to be the primary factor affecting the undrained response, whereas the influence of dilatancy parameters is considered secondary.

5 Discussion

The constitutive model presented in this paper incorporates the state-parameter dependency of elastic shear modulus and meanwhile introduces a state-parameter-dependent hardening modulus. The simulations agree reasonably well with the test results for clean and silty sand specimens under a wide range of initial states. All test data in this study were obtained from specimens reconstituted by moist tamping. The advantages of the moist tamping method include that it is able to produce specimens with a wide range of density, and it prevents segregation of coarse and fine particles [40, 41]. According to a microscopic study [43], the fabric formed by moist tamping is less anisotropic than that formed by dry deposition in terms of particle orientation. The present model does not consider the effect of fabric that is associated with particle orientation, voids and contact normal [13, 27, 43, 45].

The critical state parameters and the dilatancy parameters for silty sands are interesting issues. While some key factors that may affect the critical state parameters have been identified and some empirical relationships have been proposed [39, 41], more test data are required to improve evaluation of the critical state lines for silty sands. There is also a lack of systematic data sets for characterizing effects of fines on dilatancy parameters, while limited literature data seem to suggest that the dilatancy parameters are affected by fines content [35]. The h–ψ_0 correlation proposed in this study provides a better description of the state dependency of plastic hardening modulus and unifies the description for clean and silty sand, thus improving the model's performance. However, the linear equation is empirical and approximate and omits the possible curvature of the h–ψ_0 correlation. This may lead to deterioration of predictions for dilative behavior in some situations [23]. Future research is needed toward improving the model's capability in the above-mentioned aspects.

6 Conclusions

This paper presents a simple, critical state-based constitutive model that allows a unified modeling of the mechanical behavior of clean and silty sand. The model incorporates several important findings from recent laboratory experiments, and is calibrated using systematic data sets. The model can produce reasonable simulations for a range of behavior of silty sand under different initial states and with different fines contents. For flow type behavior, the model provides good predictions of the stress–strain response and the effective stress path. The instability state and the quasi-steady state, being two key features of undrained sand behavior, can be reasonably simulated as well. For non-flow type behavior, the simulations also agree reasonably well with the laboratory observations. The existence of phase transformation state is captured in a satisfactory way.

The proposed model successfully predicts that, under the same initial state in terms of void ratio and effective stress, the addition of fines can alter the undrained behavior of clean sand such that the response becomes more contractive as the fines content increases. Particularly, the model predicts the reduced strength and stress ratio at the undrained instability state due to increased fines content, indicating an increased liquefaction susceptibility caused by fines.

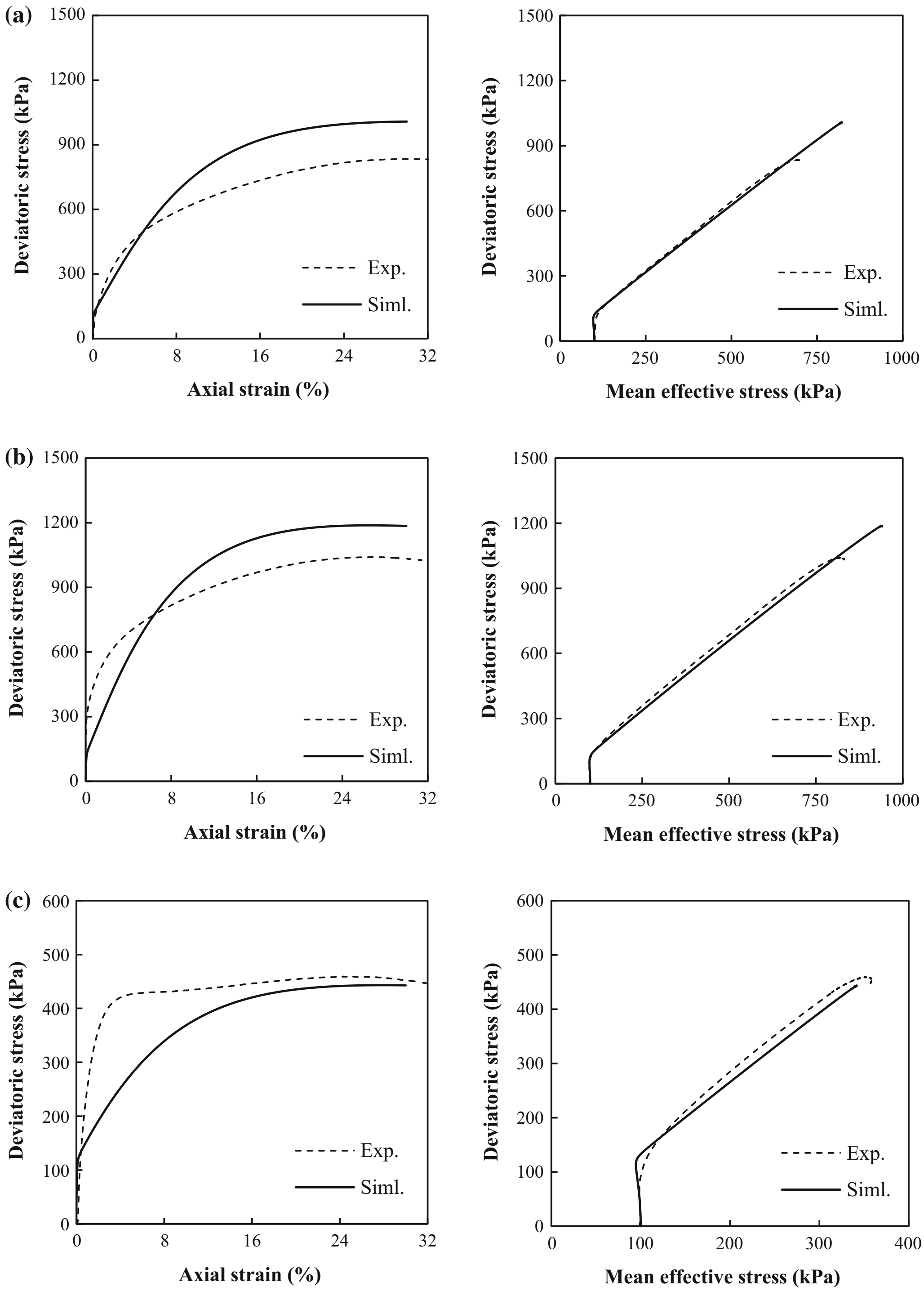

Fig. 14 Simulated non-flow type behavior of TS, TSS10 and TSS20 compared with experimental data. **a** TS-IC008, $e_c = 0.867$, $p_c' = 100$ kPa, **b** TSS10-IC006, $e_c = 0.783$, $p_c' = 100$ kPa, **c** TSS20-IC004, $e_c = 0.788$, $p_c' = 100$ kPa

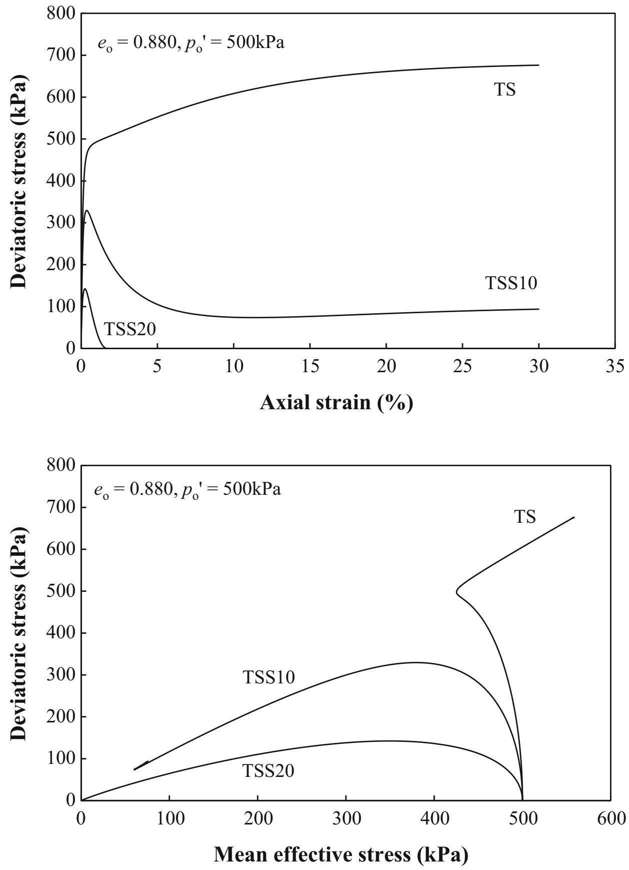

Fig. 15 Effects of fines on the undrained monotonic behavior of sand

Acknowledgements This work was supported by the Research Grants Council of Hong Kong through the General Research Fund (17250316, 17205717). This support is gratefully acknowledged.

References

1. Been K, Jefferies MG (1985) A state parameter for sands. Geotechnique 35(2):99–112
2. Borja RI, Andrade JE (2006) Critical state plasticity. Part VI: meso-scale finite element simulation of strain localization in discrete granular materials. Comput Methods Appl Mech Eng 195(37):5115–5140
3. Fuentes W, Triantafyllidis T, Lizcano A (2012) Hypoplastic model for sands with loading surface. Acta Geotech 7(3):177–192
4. Gu X, Yang J, Huang M (2013) Laboratory measurements of small strain properties of dry sands by bender element. Soils Founds 53(5):735–745
5. Guo P, Su X (2007) Shear strength, interparticle locking, and dilatancy of granular materials. Can Geotech J 44(5):579–591
6. Huang YT, Huang AB, Kuo YC, Tsai MD (2004) A laboratory study on the undrained strength of a silty sand from Central Western Taiwan. Soil Dyn Earthq Eng 24(9–10):733–743
7. Iwasaki T, Tatsuoka F (1977) Effect of grain size and grading on dynamic shear moduli of sand. Soils Founds 17(3):19–35
8. Jefferies MG (1993) Nor-Sand: a simple critical state model for sand. Geotechnique 43(1):91–103
9. Jefferies MG, Been K (2006) Soil liquefaction: a critical state approach. Taylor & Francis, London
10. Lade PV, Yamamuro JA (1997) Effects of nonplastic fines on static liquefaction of sands. Can Geotech J 34(6):918–928
11. Li XS (2002) A sand model with state-dependent dilatancy. Geotechnique 52(3):173–186
12. Li XS, Dafalias YF (2000) Dilatancy for cohesionless soils. Geotechnique 50(4):449–460
13. Li XS, Dafalias YF (2012) Anisotropic critical state theory: role of fabric. J Eng Mech 138(3):263–275
14. Li XS, Wang Y (1998) Linear representation of steady-state line for sand. J Geotech Geoenviron Eng 124(12):1215–1217
15. Liang LB (2016) Static liquefaction of sand-fines mixtures with the presence of initial shear stress, M.Phil. Thesis, The University of Hong Kong
16. Ling HI, Yang S (2006) Unified sand model based on the critical state and generalized plasticity. J Eng Mech 132(12):1380–1391
17. Manzari MT, Dafalias YF (1997) A critical state two-surface plasticity model for sands. Geotechnique 47(2):255–272
18. Murthy T, Loukidis D, Carraro J, Prezzi M, Salgado R (2007) Undrained monotonic response of clean and silty sands. Geotechnique 57(3):273–288
19. Ni Q, Tan TS, Dasari GR, Hight DW (2004) Contribution of fines to the compressive strength of mixed soils. Geotechnique 54(9):561–569
20. Papadimitriou AG, Bouckovalas GD, Dafalias YF (2001) Plasticity model for sand under small and large cyclic strains. J Geotech Geoenviron Eng 127(11):973–983
21. Pitman TD, Robertson PK, Sego DC (1994) Influence of fines on the collapse of loose sands. Can Geotech J 31(5):728–739
22. Potts DM, Zdravković L (2001) Finite element analysis in geotechnical engineering: theory. Thomas Telford, London
23. Rahman MM, Lo SCR, Dafalias YF (2014) Modelling the static liquefaction of sand with low-plasticity fines. Geotechnique 64(11):881–894
24. Simoni A, Houlsby GT (2006) The direct shear strength and dilatancy of sand–gravel mixtures. Geotech Geol Eng 24(3):523–549
25. Stamatopoulos CA, Lopez-Caballero F, Modaressi-Farahmand-Razavi A (2015) The effect of preloading on the liquefaction cyclic strength of mixtures of sand and silt. Soil Dyn Earthq Eng 78:189–200
26. Sze HY (2010) Initial shear and confining stress effects on cyclic behaviour and liquefaction resistance of sands, Ph.D. thesis. The University of Hong Kong
27. Sze H, Yang J (2014) Failure modes of sand in undrained cyclic loading: impact of sample preparation. J Geotech Geoenviron Eng 140(1):152–169
28. Taiebat M, Dafalias YF (2008) SANISAND: simple anisotropic sand plasticity model. Int J Numer Anal Methods Geomech 32(8):915–948
29. Thevanayagam S, Shenthan T, Mohan S, Liang J (2002) Undrained fragility of clean sands, silty sands, and sandy silts. J Geotech Geoenviron Eng 128(10):849–859
30. Wang G, Xie Y (2014) Modified bounding surface hypoplasticity model for sands under cyclic loading. J Eng Mech 140(1):91–101
31. Wei LM (2012) Static liquefaction and flow failure of sandy soils, Ph.D. thesis. The University of Hong Kong
32. Wichtmann T, Triantafylidis T (2009) Influence of the grain-size distribution curve of quartz sand on the small-strain shear modulus Gmax. J Geotech Geoenviron Eng ASCE 135(10):1404–1418
33. Wichtmann T, Hernandez M, Triantafylidis T (2015) On the influence of a non-cohesive fines content on small strain stiffness, modulus degradation and damping of quartz sand. Soil Dyn Earthq Eng 69:103–114

34. Wood DM (1990) Soil behaviour and critical state soil mechanics. Cambridge University Press, Cambridge
35. Xiao Y, Liu H, Chen Y, Chu J (2014) Strength and dilatancy of silty sand. J Geotech Geoenviron Eng 140(7):06014007
36. Yang J (2002) Non-uniqueness of flow liquefaction line for loose sand. Geotechnique 52(10):757–760
37. Yang J, Li X (2004) State-dependent strength of sands from the perspective of unified modeling. J Geotech Geoenviron Eng 130(2):186–198
38. Yang J, Liu X (2016) Shear wave velocity and stiffness of sand: the role of non-plastic fines. Geotechnique 66(6):500–514
39. Yang J, Luo XD (2015) Exploring the relationship between critical state and particle shape for granular materials. J Mech Phys Solids 84:196–213
40. Yang J, Sze HY (2011) Cyclic behaviour and resistance of saturated sand under non-symmetrical loading conditions. Geotechnique 61(1):59–73
41. Yang J, Wei LM (2012) Collapse of loose sand with the addition of fines: the role of particle shape. Geotechnique 62(12):1111–1125
42. Yang J, Wei LM, Dai BB (2015) State variables for silty sands: global void ratio or skeleton void ratio? Soils Founds 55(1):99–111
43. Yang Z, Li X, Yang J (2008) Quantifying and modelling fabric anisotropy of granular soils. Geotechnique 58(4):237–248
44. Zhang JM, Wang G (2012) Large post-liquefaction deformation of sand, part I: physical mechanism, constitutive description and numerical algorithm. Acta Geotech 7(2):69–113
45. Zhao J, Gao Z (2016) Unified anisotropic elastoplastic model for sand. J Eng Mech 142(1):04015056
46. Zlatović S, Ishihara K (1995) On the influence of nonplastic fines on residual strength. In: Proceedings of the 1st international conference earthquake geotechnical engineering, Tokyo, pp 239–24

Publisher's Note